

Spectral and spatial decomposition of lithospheric magnetic field models using spherical Slepian functions

Ciarán D. Beggan¹, Jarno Saarimäki^{2*}, Kathryn A. Whaler² and Frederik J. Simons³

¹*British Geological Survey, Murchison House, West Mains Road, Edinburgh EH9 3LA, UK. Email: ciar@bgs.ac.uk*

²*School of GeoSciences, University of Edinburgh, West Mains Road, Edinburgh EH9 3JW, UK.*

³*Department of Geosciences, Princeton University, Guyot Hall, Princeton NJ 08544, USA.*

published 15 February 2013

SUMMARY

Global magnetic field models are typically expressed as spherical-harmonic expansion coefficients. Slepian functions are linear combinations of spherical harmonics that produce new basis functions which vanish approximately outside chosen geographical boundaries, but also remain orthogonal within the spatial region of interest. Hence, they are suitable for decomposing spherical-harmonic models into portions that have significant magnetic field strength only in selected areas. Slepian functions are spatio-spectrally concentrated, balancing spatial bias and spectral leakage. Here, we employ them as a basis to decompose the global lithospheric magnetic field model MF7 up to degree and order 72, into two distinct regions. One of the resultant fields is concentrated within the ensemble of continental domains, and the other is localised over its complement, the oceans. Our procedure neatly divides the spectral power at each harmonic degree into two parts. The field over the continents dominates the overall crustal magnetic field, and each region has a distinct power spectral signature. The oceanic power spectrum is approximately flat, while that of the continental region shows increasing power as the spherical-harmonic degree increases. We provide a further breakdown of the field into smaller, non-overlapping continental and oceanic regions, and speculate on the source of the variability in their spectral signatures.

18 **Key words:** Magnetic anomalies: modelling and interpretation; Satellite magnetics

19 **1 INTRODUCTION**

20 The magnetic field of Earth is one of the few measurable quantities that provide remote access to
21 the internal dynamics of our planet (see, e.g. Thébaud et al. 2010). For instance, past movements
22 of tectonic plates may be inferred from the orientation of magnetic minerals in the crust, while the
23 secular variation of the field at the surface gives insight into the properties of the outer core (Hulot
24 et al. 2010).

25 This paper studies the global lithospheric magnetic field at Earth's surface, focusing on the
26 different signatures of the field over continents and oceans. On short time scales, the crustal field
27 can be regarded as effectively constant in time, though its induced part does vary slightly (Thébaud
28 et al. 2009, 2010). The magnitude of the crustal field can vary from a fraction of a nanoTesla (nT)
29 to thousands of nT at Earth's surface. The continents comprise a number of ancient blocks with
30 varying magnetic properties, while the oceanic crust is relatively young, thinner, and appears much
31 more homogeneous (Arkani-Hamed & Dymant 1996). It is generally assumed that at a global
32 scale the continental regions mainly exhibit induced magnetisation while the oceanic regions can
33 contain both remanent and induced magnetisation (Cohen & Achache 1994; Dymant & Arkani-
34 Hamed 1998). One manifestation of the remanent magnetisation of the ocean floor is the "striping"
35 parallel to mid-ocean ridges, which is due to past reversals of the magnetic poles. The width of
36 the stripes, from a few kilometres to tens of kilometres, reflects the combination of plate spreading
37 rate and reversal frequency (Kono 2007).

38 Since the times of Gauss, planetary magnetic fields have been represented by the expansion
39 of the potential in the basis of spherical harmonics (e.g. Backus et al. 1996; Langel & Hinze
40 1998). From the 'spectral' representation in terms of spherical-harmonic 'Gauss' coefficients at
41 individual degrees and orders, regional 'spatial' properties are difficult to deduce. The spherical
42 harmonics are perfectly localised spectrally (Freedman & Michel 1999), but their spatial energy is

* Now at Astroock Geophysics, Finland.

43 geographically distributed over the entire globe. Information about the field contained in a single
44 spherical-harmonic coefficient thus ultimately derives from signal that may originate anywhere
45 on the surface of the planet. Only by expanding the entire set of spherical harmonics back into
46 the space domain do we regain a sense of the geographic distribution of the field — at the price
47 of confounding its spectral properties. The situation is even worse when the spherical-harmonic
48 coefficients are squared (which removes phase information) and summed over all orders, to report
49 a (by this construction necessarily) isotropic ‘power spectrum’ or ‘degree variance’, at each indi-
50 vidual degree. Here too, while we get an idea of the mean-squared value of the field at a certain
51 spherical-harmonic degree, we remain ignorant of the distribution of precisely where, geograph-
52 ically, the field is prominently contributing to the power at that degree. In other words, spherical
53 harmonics form a well-understood and convenient apparatus for the representation and analysis of
54 magnetic fields globally, but they lack the flexibility to identify the spatial and spectral structure
55 of such fields from ‘spatio-spectrally’ mixed vantage point.

56 One of the early attempts at bringing spatial selectivity to spherical-harmonic based repre-
57 sentations involved an approach reminiscent of ‘wavelet’ analysis (Simons et al. 1997). Spatially
58 selective windows targeting a particular spectral degree range were designed, and a space-spectral
59 analysis conducted via a convolutional approach. The drawback of wavelets and their relatives
60 is that the area of the spatial region over which information is being extracted scales inversely
61 with the spherical-harmonic degree range of interest. Large-degree (high spatial frequency) infor-
62 mation derives from small areas, small-degree (low spatial frequency) structure is obtained from
63 larger regions.

64 In order to study the spectral behavior of a geophysical signal confined to a particular geo-
65 graphic region of interest, a different solution must be sought. Suppose we were to window the
66 data over a spatial region of interest using a simple multiplicative binary mask (e.g. Peebles 1973;
67 Wandelt et al. 2001; Dahlen & Simons 2008). In the spectral domain, this operation would es-
68 sentially correspond to a convolution of the spherical-harmonic expansion coefficients of the data
69 with those of the mask itself. A binary mask, while perfectly localised in the space domain, has an
70 infinitely-dimensional ringing behavior in the spectral domain. The analysis operation would thus

71 lead to results displaying undesirable spectral-domain artifacts. Evidently some way of ‘tapering’
72 the ‘boxcar’ must be found, by which some spatial selectivity is sacrificed in return for spectral
73 windows that have better sidelobe behavior (Tegmark 1996, 1997). Such procedures, known as
74 ‘apodisation’, were first cast as an optimisation problem for application to time-series analysis in
75 the 1960s (see, e.g., Slepian 1983).

76 With spherical Slepian functions (Wieczorek & Simons 2005; Simons et al. 2006) the trade-
77 off between spectral and spatial concentration on the surface of the unit sphere is optimised, by
78 constructing a particular linear combination of spherical harmonics. This combination is such that
79 while bandlimited within a certain spectral interval of interest, the functions maximise their spatial
80 energy over a certain spatial region of interest, preserving orthogonality over the entire sphere
81 as well as over the chosen spatial domain. The trade-off arises because bandlimited expansions
82 cannot be spatially limited, nor vice versa, which is a consequence of the Paley-Wiener theorem
83 (Daubechies 1992; Mallat 1998), and because spatial concentration is inversely proportional to
84 spectral concentration, which is a consequence of the Heisenberg inequality (Percival & Walden
85 1993; Narcowich & Ward 1996; Freedon & Michel 1999; Wieczorek & Simons 2005).

86 Only one Slepian function is the spatially ‘best’-concentrated function for a given target re-
87 gion R on the surface of the sphere Ω . The complete solution to the ‘concentration problem’ as
88 put forth by Simons et al. (2006) contains an entire basis set of functions which are eigenfunc-
89 tions of the spatio-spectral localisation (bandlimitation followed by spatial limitation) projection
90 operator. These eigenfunctions are all orthogonal to each other over the region R , which can have
91 an arbitrarily complex shape, and they are furthermore also orthogonal over the entire globe Ω .
92 The eigenvalues embody the level to which the energy of the spatial functions is confined to the
93 region of interest R . Well-concentrated functions are ‘large’ within the region and have eigen-
94 values close to one. These can be used to approximate bandlimited signals inside the region of
95 interest. The rest of the set consists of poorly-concentrated, nearly-zero-eigenvalue functions that
96 are ‘small’ within R but large in the complementary region $\Omega \setminus R$. Those functions are suitable for
97 approximating bandlimited signals outside the spatial region of primary interest.

98 Taken together, the Slepian basis set is merely a unitary linear transformation of the spherical-

99 harmonic basis, but it is the spatial region of interest built into their construction via quadratic
100 maximisation that leads to their efficiency for modelling regional signals. A small subset is ‘large’
101 in the region R , the vast majority is ‘small’ over R . The double orthogonality of the Slepian func-
102 tions, both over R and over $\Omega \setminus R$ is a property that is convenient and very welcome on statistical
103 grounds, e.g. when inversions for the source or estimations of the power spectral density of the
104 field components or the overall potential are being made on the basis of actual satellite data (Si-
105 mons & Dahlen 2006; Dahlen & Simons 2008; Simons et al. 2009; Plattner & Simons 2012), but
106 note no such attempts are being made here. It finally should be stated that other data-based inver-
107 sion approaches may provide the desired (double) orthogonality of the basis functions (e.g. Hwang
108 1993; Górski 1994; Xu 1998; Schachtschneider et al. 2010; Slobbe et al. 2012; Schachtschneider
109 et al. 2012), but Slepian functions are the only ones that achieve this feat in a fully analytical, and
110 easily computable framework, from prior considerations of the geometry of the region of interest
111 or data availability.

112 In summary, and relating back to the objective in this paper, which is to study the spectral sig-
113 nature of the Earth’s magnetic field over continents and oceans separately, the Slepian functions
114 provide an optimal basis, or else, a set of windowing functions, to model, analyse or represent,
115 the magnetic potential within non-overlapping geographical regions. In a decomposition where
116 the entire bandwidth of the original model is being used, but selectively truncated expansions into
117 Slepian functions are formed from the original spherical-harmonic coefficients, the fit of the signal
118 within individual geographical regions is effectively maximised, while at the same time, edge ef-
119 fects, which lead to distortions in their spherical-harmonic representations, are minimised. Council
120 et al. (1991) demonstrated that differences between the field in continental and oceanic crust mod-
121 elled exclusively using spherical harmonic functions may be influenced by edge effects. Using
122 Slepian functions, global signals can be decomposed into effectively regional models that best
123 approximate and thus separate the field over the areas of interest, and whose spherical-harmonic
124 spectrum can be studied robustly. Ultimately, our objective should be to use the separation of the
125 magnetic fields over the continents and oceans for geological inference into the magnetisation

126 structure of the respective domains (e.g. Gubbins et al. 2011), but this goal remains out of the
127 scope of the present contribution.

128 The Slepian decomposition method can be applied to magnetic fields from other planetary
129 bodies with sufficient spherical-harmonic model resolution and identifiable regions of interest. The
130 technique can also be used in other areas where spatial data are commonly described by spherical
131 harmonics such as ocean or glacial signals in gravity models (e.g. Reigber et al. 2005; Slobbe et al.
132 2012; Harig & Simons 2012) or when interpreting seismic shear wave velocity models (e.g. Becker
133 & Boschi 2002; Ritsema et al. 2010), but also astrophysics (e.g. Peebles 1973; Hauser & Peebles
134 1973) and cosmology (e.g. Tegmark 1997; Oh et al. 1999).

135 Regional modelling can be achieved by other methods, such as via harmonic splines (Shure
136 et al. 1982, 1985; Amirbekyan et al. 2008), (Revised) Spherical Harmonic Cap Analysis (Haines
137 1985; Thébault et al. 2006) and various other localising techniques including wavelets (e.g. Holschnei-
138 der et al. 2003; Lesur 2006). Each method has advantages over global spherical-harmonic analysis
139 for local regions. Schott & Thébault (2011) discuss the merits and limitations of each approach in
140 detail. However, none of the above techniques attempts to formally optimise field separation over
141 arbitrary regions with irregular boundaries from a global model consisting of spherical-harmonic
142 coefficients. In this respect the approach by Slepian functions is unique and suited to the prob-
143 lem of studying the contributions to the global spherical-harmonic power spectrum that arise from
144 distinct geographic regions, continents and oceans, and to assess their spectral characteristics in-
145 dividually.

146 Several high-quality lithospheric field models are available for study. Much use has been made
147 of the excellent satellite vector data from the Ørsted, Champ and SAC-C missions which operated
148 between 1999 and 2010. Models of the lithospheric field include satellite-only models such as
149 MEME (Thomson et al. 2010) and POMME7 (Maus et al. 2010), and models including data from
150 surface, marine, and aeromagnetic surveys such as EMAG2 (Maus et al. 2009). The spherical-
151 harmonic expansion coefficients of these lithospheric models (the “Gauss coefficients”) typically
152 agree to about degree 80. We restrict our study to the crustal field between spherical harmonic
153 degrees 16–72 using the Gauss coefficients from the MF7 model (Maus et al. 2007). Further im-

154 improvements to lithospheric field models are anticipated with data from the ESA Swarm satellite
155 mission (Friis-Christensen et al. 2006).

156 We use a spherical Slepian-function decomposition of the field over the continents and their
157 complement, the oceans, to investigate the differences between the field over those regions that
158 can be identified from the spherical-harmonic power spectra. In Section 2 we review some basics
159 of the spherical Slepian-function decomposition and establish the framework for its description.
160 Originally developed as low-pass bandlimited functions, we also describe a decomposition using
161 band-pass Slepian functions. For both of these we demonstrate how to decompose a field model of
162 Gauss coefficients into separate regions. In Section 3, we present the results for the crustal mag-
163 netic field with an analysis of the trade-off between spatial and spectral accuracy that arises from
164 the coupling between each region. In Section 4 we discuss our findings and Section 5 concludes
165 the paper.

166 2 METHODOLOGY

167 Before we proceed, we should caution the reader that history has decided that the commonly used
168 symbol for the scalar Gauss expansion coefficients of the potential at spherical-harmonic degree l
169 and order m should be g_l^m .

170 In more recent history (e.g. Simons et al. 2006; Simons & Dahlen 2006), we have used $g_\alpha(\theta, \phi)$
171 for the α th bandlimited scalar Slepian function evaluated at colatitude θ and longitude ϕ on the unit
172 sphere, and $g_{\alpha,lm}$ for the expansion coefficients of the Slepian functions in the spherical-harmonic
173 basis. When we collect the coefficients $g_{\alpha,lm}$ for the α th Slepian functions into a (column) vector,
174 we write \mathbf{g}_α , when we collect the expansion coefficients of all of the Slepian functions, column
175 by column, in to a matrix, we write the results as \mathbf{G} , and when we collect the Slepian functions
176 themselves, evaluated as a function of colatitude and longitude, into a column vector, we write
177 $\mathbf{g}(\theta, \phi)$.

178 At the risk of antagonising our forebears we shall use v_l^m for the (Gauss) expansion coefficients
179 of the potential V , and collect them in a column vector \mathbf{v} .

180 **2.1 Spherical harmonics**

Magnetic fields originating inside or outside Earth can be approximated by a scalar potential V that satisfies Laplace's equation,

$$\nabla^2 V = 0, \quad (1)$$

i. e., is harmonic, outside the source region. From this potential, the magnetic field \mathbf{B} is obtained by

$$\mathbf{B} = -\nabla V. \quad (2)$$

In spherical coordinates (r, θ, ϕ) the harmonic potential of the internal field is conveniently represented by a spherical-harmonic expansion to a certain bandwidth L ,

$$V(r, \theta, \phi) = a \sum_{l=1}^L \left(\frac{a}{r}\right)^{l+1} \sum_{m=-l}^l v_l^m Y_l^m(\theta, \phi), \quad (3)$$

181 where $Y_l^m(\theta, \phi)$ is a real spherical surface harmonic of degree l and order m , the Gauss coeffi-
 182 cients v_l^m define the weightings of the individual harmonics, and a is a reference radius for the
 183 expansion (typically Earth's mean radius, 6371.2 km), which is valid when $r \geq a$. Here, the v_l^m
 184 and v_l^{-m} replace the g_l^m and h_l^m in the traditional geomagnetic notations.

Spherical surface harmonics are orthogonal over the whole sphere Ω : when $l \neq l'$ or $m \neq m'$,

$$\int_{\Omega} Y_l^m(\theta, \phi) Y_{l'}^{m'}(\theta, \phi) d\Omega = 0. \quad (4)$$

In geomagnetism, the normalisation (i. e. the nonzero value of eq. 4 when $l = l'$ and $m = m'$) is usually that due to Schmidt (see Blakely 1996). The spherical-harmonic power spectrum R_l is then defined as the squared magnitude of the magnetic field at degree l averaged over a spherical surface of radius r , which, in this Schmidt normalisation, amounts to (Mauersberger 1956; Lowes 1966, 1974; Sabaka et al. 2010):

$$R_l(r) = (l + 1) \left(\frac{a}{r}\right)^{2l+4} \sum_{m=-l}^l (v_l^m)^2. \quad (5)$$

185 We do not speak of “spectral densities” since we do not report averages per spherical-harmonic
 186 degree, but rather totals. A “flat” power spectrum in the sense of eq. (5) is not “white”, as “white-
 187 ness” would imply that the spatial autocorrelation is a delta function (Dahlen & Simons 2008,

188 their eqs 33–34). It is important to heed the implications of this particular definition for a physical
 189 interpretation (Hipkin 2001; Maus 2008).

190 2.2 Slepian functions

191 2.2.1 Notation and objective

192 Spherical surface harmonics are functions of global support that can be converted, by a unitary
 193 linear transformation, into a spherical Slepian basis whose energy is concentrated onto specific
 194 patches of the sphere (Wieczorek & Simons 2005; Simons et al. 2006). A detailed review of
 195 the construction and properties of 1D, 2D and 3D Slepian functions is given by Simons (2010).
 196 Here, we present a slightly different notation from that previously used by these authors. Both
 197 notations are equivalent, but in this paper we rely more on vector-matrix operations than on the
 198 explicit summations that have been mostly used elsewhere. First, we consider some elementary
 199 mathematical definitions.

To allow for computations other than in geomagnetism, we include the $l = 0$ monopole term
 in what follows below. Spherical surface harmonics up to degree and order L can be expressed as
 a vector of $(L + 1)^2$ elements, each of which is a function of position (θ, ϕ) on the unit sphere:

$$\mathbf{y}(\theta, \phi) = \left[Y_0^0(\theta, \phi) \cdots Y_l^m(\theta, \phi) \cdots Y_L^L(\theta, \phi) \right]^T. \quad (6)$$

200 The ordering of the spherical harmonics Y_l^m is naturally arbitrary. The notation is such that all
 201 boldface lower-case characters represent column vectors and boldface upper-case represents ma-
 202 trices. In geomagnetism, the monopole harmonic (Y_0^0) is usually ignored (or set to zero), but we
 203 include it in this analysis to prevent loss of generality for other applications.

On a unit sphere, the potential $V(\theta, \phi)$ up to degree L is represented in a spherical-harmonic
 basis by a single $(L + 1)^2$ -dimensional column vector of Gauss coefficients, \mathbf{v} . The potential on
 the surface is obtained from these Gauss coefficients as

$$V(\theta, \phi) = \mathbf{v}^T \mathbf{y}(\theta, \phi) = \mathbf{v} \cdot \mathbf{y}(\theta, \phi). \quad (7)$$

204 The representation of the potential in a spherical-harmonic spectral-domain basis by the lower-

205 case boldface symbol \mathbf{v} which lacks a dependence on (θ, ϕ) distinguishes it from the space-domain
 206 potential $V(\theta, \phi)$ in our notation.

Spherical Slepian functions (hereafter simply: Slepian functions) are an alternative basis,

$$\mathbf{g}(\theta, \phi) = \left[g_1(\theta, \phi) \cdots g_\alpha(\theta, \phi) \cdots g_{(L+1)^2}(\theta, \phi) \right]^T. \quad (8)$$

Each of the entries in eq. (8) is a basis function that is linearly related to the surface harmonics by the expansion

$$g_\alpha(\theta, \phi) = \mathbf{g}_\alpha^T \mathbf{y}(\theta, \phi) = \mathbf{g}_\alpha \cdot \mathbf{y}(\theta, \phi). \quad (9)$$

As in eq. (7), our notation distinguishes the spatial-domain Slepian functions $g_\alpha(\theta, \phi)$ from their expansion coefficients \mathbf{g}_α in the spherical-harmonic basis. Slepian basis functions are orthonormal over the unit sphere so that

$$\mathbf{g}_\alpha \cdot \mathbf{g}_{\alpha'} = \begin{cases} 1 & \text{if } \alpha = \alpha', \\ 0 & \text{otherwise.} \end{cases} \quad (10)$$

The Slepian basis $\mathbf{g}(\theta, \phi)$ is produced from the spherical surface harmonic basis $\mathbf{y}(\theta, \phi)$ by multiplying the latter by the unitary matrix which is given by

$$\mathbf{G}^T = \begin{bmatrix} \mathbf{g}_1^T \\ \vdots \\ \mathbf{g}_{(L+1)^2}^T \end{bmatrix}, \quad \mathbf{G} \mathbf{G}^T = \mathbf{I}. \quad (11)$$

207 The matrix \mathbf{G} is constructed by optimisation, as will be shown in the next section (2.2.2), to
 208 localise the solution over specified areas or regions (and their complements), for a given band-
 209 width L . Note that the regions of interest do not have to be connected or contiguous, but they
 210 must be non-overlapping to preserve orthogonality between different constructions. For the case
 211 of unconnected continental regions on Earth, and the complementary oceanic domain, a single
 212 optimisation procedure determines a complete set of basis functions which naturally separate into

213 those basis functions that are well localised over either of the two distinct domains:

$$\begin{aligned}
 \mathbf{G}^T \mathbf{y}(\theta, \phi) &= \begin{bmatrix} \mathbf{G}_{\text{in}}^T \mathbf{y}(\theta, \phi) \\ \mathbf{G}_{\text{out}}^T \mathbf{y}(\theta, \phi) \end{bmatrix} = \begin{bmatrix} g_1(\theta, \phi) \\ \vdots \\ g_K(\theta, \phi) \\ g_{K+1}(\theta, \phi) \\ \vdots \\ g_{(L+1)^2}(\theta, \phi) \end{bmatrix} \\
 &= \begin{bmatrix} \mathbf{g}_{\text{in}}(\theta, \phi) \\ \mathbf{g}_{\text{out}}(\theta, \phi) \end{bmatrix}, \tag{12}
 \end{aligned}$$

214 where the index K denotes the last element of the functions primarily concentrated in the first
 215 domain, subscripted “in” (that is, inside the region of interest), and $K + 1$ denotes the first element
 216 of the functions concentrated in the other domain, subscripted “out” (outside the region of interest,
 217 inside of the complement). The basis functions of domain “in” are approximately non-zero only
 218 within the chosen region R , while those of domain “out” are concentrated outside R . The value
 219 of K depends on the bandwidth and the fractional area of the “in” region. With this type of a
 220 spherical harmonic-to-Slepian transformation we restrict ourselves to analysing only one spherical
 221 shell (e. g. the surface) at a time. Simons & Dahlen (2006, their Section 6.3) discuss aspects of
 222 harmonic continuation using the Slepian basis.

223 2.2.2 Determination of the Slepian basis

224 The Slepian functions span a linear subspace of $\mathbf{y}(\theta, \phi)$ in which the energy, or sum-squared
 225 function value over R , is maximised. At this point the geometry of the region under consideration
 226 enters the calculation. We compute the Gram matrix of energy in R as

$$\mathbf{D} = \int_R \mathbf{y}(\theta, \phi) \mathbf{y}^T(\theta, \phi) d\Omega \tag{13}$$

$$= \int_R \begin{bmatrix} Y_0^0 Y_0^0 & \cdots & Y_0^0 Y_L^L \\ \vdots & \ddots & \vdots \\ Y_0^0 Y_L^L & \cdots & Y_L^L Y_L^L \end{bmatrix} d\Omega. \tag{14}$$

This “localisation” matrix is symmetric and the subspace of maximum energy is readily obtained by eigenvalue decomposition. The eigenvalues and eigenvectors of \mathbf{D} are defined as

$$\mathbf{D}\mathbf{G} = \mathbf{G}\mathbf{\Lambda}, \quad (15)$$

where each column of \mathbf{G} contains one eigenvector and $\mathbf{\Lambda}$ is a diagonal matrix with the corresponding eigenvalues

$$\mathbf{\Lambda} = \text{diag}(\lambda_1, \dots, \lambda_\alpha, \dots, \lambda_{(L+1)^2}). \quad (16)$$

227 The symmetry of \mathbf{D} provides that all eigenvalues are real and positive (or zero) and that all eigen-
 228 vectors are orthogonal, which makes \mathbf{G} unitary. Furthermore, each eigenvalue λ_α defines the frac-
 229 tional energy (over R compared to Ω) that is represented in the projection $g_\alpha(\theta, \phi) = \mathbf{g}_\alpha \cdot \mathbf{y}(\theta, \phi)$.
 230 The eigenvalue problem (15) is equivalent to the maximisation of λ for functions given the avail-
 231 able bandwidth L . The Slepian functions in this discussion have been perfectly bandlimited spec-
 232 trally, to degree and order L .

233 The eigenvalues λ_α are characterised by a spectrum of near-unity values separated from near-
 234 zero values by a narrow transition region. This shape is the motivation for the heuristic decomposi-
 235 tion into K “in” and $(L+1)^2 - K$ “out” functions, where $\lambda_K \approx 0.5$. It is generally not possible to
 236 separate perfectly the energy of the functions that concentrate inside and outside R in this manner.
 237 Hence, there will be spatial leakage between the two domains “in” and “out”, and the energy of
 238 the leakage depends on the eigenvalues, which are close to (but smaller than) one, $\lambda_\alpha \lesssim 1$, when
 239 $\alpha \leq K$, and greater than (but close to) zero, $\lambda_\alpha \gtrsim 0$, when $\alpha > K$.

240 The diagonalisation is reminiscent of Principal-Component Analysis (PCA) (e.g. Jolliffe 2002)
 241 with the exception that PCA traditionally finds linear subspaces that concentrate data variance
 242 rather than basis-function energy. Slepian eigenvectors and eigenvalues can also be considered
 243 to result from singular-value decomposition (SVD) if we consider the integral in (14) as a “nor-
 244 mal” matrix, the product of a matrix and its transpose, as arises in inversion problems (Simons
 245 2010). The elements of \mathbf{D} are to be evaluated by numerical integration or analytically in certain
 246 circumstances; see Wieczorek & Simons (2005) and Simons et al. (2006, 2009). When the region
 247 of concentration has the symmetry of a polar cap or an antipodal pair of polar caps (Simons &

248 Dahlen 2006), the matrix \mathbf{G} can be found without the intermediary of \mathbf{D} , through commutation
 249 relations. Numerically, this property is very attractive.

The eigenvalues λ_α cannot exceed unity because no orthonormal projection can provide more fractional energy than any of the spherical surface harmonics over the whole sphere. For eigenvalues near one, most of the energy of the projection is contained within R . When the eigenvalues are near zero, most energy of the projection is contained outside R . The sum of the eigenvalues λ_α gives the ‘‘Shannon number’’ (Simons et al. 2006), which can directly be computed from

$$K = (L + 1)^2 \frac{A}{4\pi}, \quad (17)$$

250 where A is the surface area (in steradians) of R . The Shannon number, a space-bandwidth product,
 251 approximates the dimension of the space of approximately space- (to R) and band- (to L) limited
 252 functions on the sphere. It corresponds to the number of functions that usefully project the energy
 253 of the spherical harmonics onto the target region R .

It is reasonable to omit certain spherical-harmonic degrees from the Slepian functions if there is no energy in those degrees. For instance, in crustal field models, due to the inability to separate the dominant core field contribution at degrees $l = 12\text{--}15$, Gauss coefficients of degrees $l < l_0 = 15$ are generally set to zero. In such a case, the corresponding Slepian basis (8) has $(L + 1)^2 - l_0^2$ elements and the Shannon number, modified after (17), would be

$$K = [(L + 1)^2 - l_0^2] \frac{A}{4\pi}. \quad (18)$$

254 There are corresponding changes in all related equations that refer explicitly to the dimensions of
 255 vectors and matrices, which are, however, straightforward to adapt. The resulting models would
 256 thus be based on band-pass Slepian functions rather than the low-pass ones which have been the
 257 subject of all previous work using spherical Slepian functions known to us.

258 *2.2.3 Decomposition of the Gauss coefficients*

259 A harmonic potential $V(\theta, \phi)$ can thus be decomposed into parts (almost) localised inside and
 260 outside a region R as follows:

$$V_{\text{in}}(\theta, \phi) = (\mathbf{G}_{\text{in}}^T \mathbf{v})^T \mathbf{g}_{\text{in}}(\theta, \phi), \quad (19)$$

$$V_{\text{out}}(\theta, \phi) = (\mathbf{G}_{\text{out}}^T \mathbf{v})^T \mathbf{g}_{\text{out}}(\theta, \phi). \quad (20)$$

The potential over the entire sphere is a superposition of these partial expansions,

$$V(\theta, \phi) = V_{\text{in}}(\theta, \phi) + V_{\text{out}}(\theta, \phi). \quad (21)$$

261 Furthermore, the spherical-harmonic representations of the two regional potentials become the
 262 projections

$$\mathbf{v}_{\text{in}} = (\mathbf{G}_{\text{in}} \mathbf{G}_{\text{in}}^T) \mathbf{v}, \quad (22)$$

$$\mathbf{v}_{\text{out}} = (\mathbf{G}_{\text{out}} \mathbf{G}_{\text{out}}^T) \mathbf{v}. \quad (23)$$

263 Eqs (22)–(23) imply a transfer of energy from each of the spherical-harmonic elements in the
 264 original to the individual regional expansions, although the matrices $(\mathbf{G}_{\text{in}} \mathbf{G}_{\text{in}}^T)$ and $(\mathbf{G}_{\text{out}} \mathbf{G}_{\text{out}}^T)$ are
 265 diagonally dominant. There is a trade-off between the spectral coupling and the spatial leakage
 266 from one domain to another: decreasing the amount of coupling will tend to increase the spatial
 267 bias by reducing the regional selectivity of the decomposition. The behaviour can be understood
 268 on the basis of the detailed considerations made by Simons & Dahlen (2006) for the case where
 269 linear functionals of the data result in signal estimation from noisy and incomplete observations,
 270 and by Dahlen & Simons (2008) which treated the case where quadratic data functionals result in
 271 direct estimates of the power spectral density from similar observations. There are more connec-
 272 tions implicit in the early theoretical work by Kaula (1967), Spencer & Gubbins (1980), Whaler &
 273 Gubbins (1981), and in the practical studies by Slobbe et al. (2012), Trampert & Snieder (1996),
 274 Schachtschneider et al. (2010), to name a few examples from geodesy, seismology, and geomag-
 275 netism, respectively. However, the material in this section (2.2.3) does not appear explicitly in
 276 those papers, nor has the algorithm proposed in the next section (2.2.4) been applied before.

277 2.2.4 Algorithm

278 We have implemented the ocean-continent magnetic-field decomposition using the following five
279 algorithmic steps for which we have made the computer code freely available:

280 (i) A file containing the latitudes and longitudes of the boundary outlines was generated to
281 determine the spatial region of interest R . The average spacing between points was approximately
282 10 km.

283 (ii) A localisation matrix \mathbf{D} was computed for the region of interest on the sphere using eq. (14)
284 with the bandwidth $L = 72$. This is most the time-consuming step, which, however, benefited from
285 a parallel implementation which reduced computation time to a matter of minutes on a contempo-
286 rary eight-processor machine.

287 (iii) Slepian basis functions for the region were generated using the eigenvector decomposition
288 of the localisation matrix of eq. (15). They were sorted by eigenvalue, from the largest to the
289 smallest.

290 (iv) The spherical-harmonic coefficients were converted into equivalent Slepian coefficients
291 using eqs (19)–(20).

292 (v) The Shannon number K was used to separate the Slepian coefficients into the two com-
293plementary regions of interest, and the Slepian coefficients were transformed back to spherical-
294harmonic coefficients using eqs (22)–(23).

295 The spherical-harmonic coefficients for each region can be treated as usual, for example, to find
296 field components at a series of points for plotting in map form, or squared, summed and scaled
297 to give a power spectrum as per eq. (5). With regards to this last operation, it is to be noted
298 that this does not amount to a “multitaper” power spectral estimate in the sense of Wieczorek
299 & Simons (2007) or Dahlen & Simons (2008, their eqs 130 and 139). In the present approach
300 we focused on containing spatial bias by achieving field separability over both regions at the full
301 resolution of the data. As shown in the previous section (2.2.3) and in the examples to follow, this
302 leads to a spectral coupling with a manageable bias, or effective bandwidth of resolution, for the
303 spectral estimate, whose variance, unlike in both studies cited, we did not attempt to minimise. The

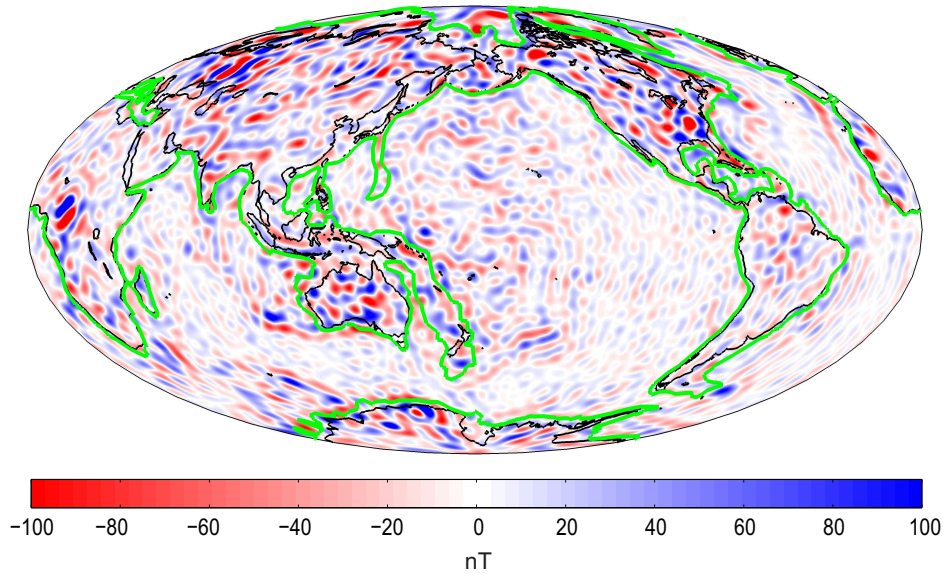


Figure 1. The radial component of the crustal magnetic field MF7 (Maus et al. 2007) for the spherical harmonic degrees $l = 16-72$ (units: nT). The green line shows the continental crust boundaries and the black line denotes the shorelines for reference. The colour scale is saturated: the field values reach a minimum of -288 nT and a maximum of 397 nT in places.

304 advantage of our present approach is that it stays intuitively close to geomagnetic practice while
 305 alleviating the drawbacks of forming “periodogram” spectral estimates with simple binary masks
 306 for the continents and the oceans — a case treated in detail by Dahlen & Simons (2008, their
 307 Section 5). Field separation and spectral estimation are different statistical problems, one linear
 308 in the data and the other quadratic: our approach of basis projection, truncation, and reprojection,
 309 for evaluation in the space domain and spectral estimation, serves a dual purpose that is closer in
 310 spirit to the former, without excessively violating the basic premise of the latter. Lewis & Simons
 311 (2012) can be consulted for an example for the Martian lithospheric field, where the focus lies on
 312 the estimation and parameterised inversion of the power spectrum rather than on separable field
 313 representation with the quadratic spectrum as a by-product, as is our case.

314 **3 CRUSTAL FIELD DECOMPOSITION**

315 The lithospheric field decomposed is the model MF7 of Maus et al. (2007), which extends to
 316 spherical harmonic degree 133. This model, derived for use at the Earth’s mean radius (6371.2 km),

317 is based on Champ satellite measurements up to April 2010. The model is suitable for the analysis
 318 of long-wavelength features of the lithospheric field, as shorter wavelengths become distorted due
 319 to data processing and model regularisation. We thus examine the field at the spherical-harmonic
 320 degrees $l = 16-72$, as degrees beyond 72 are subject to along-track filtering of the data and stronger
 321 *a priori* smoothing (Maus et al. 2008). The boundaries of the continental crust are approximated
 322 from global relief images of the NOAA ETOPO2v2 map. In most regions these images show clear
 323 features at the edges of continental and oceanic regions, which can be confirmed by comparison
 324 with oceanic crust boundaries of Müller et al. (2008) or Counil et al. (1991) among others.

325 Fig. 1 shows the radial component of the magnetic field of MF7 along with the continental
 326 boundaries. We employ Slepian functions to decompose the scalar potential into a continental do-
 327 main and its complement, the oceanic domain. The figure includes the shoreline as a reference so
 328 that submarine continental crust is also distinguishable. We use the radial component of the mag-
 329 netic field to assess the decompositions visually in the following sections. We analyse the results
 330 by studying spherical-harmonic power spectra (eq. 5), even though the optimal decomposition of
 331 the potential is not necessarily also optimal for its field components (Plattner et al. 2012). The
 332 number of Slepian eigenfunctions and their eigenvalues for each region are computed using the
 333 appropriate Shannon numbers from eqs (17) or (18). Some large-scale lithospheric anomalies are
 334 missing from the model, because the lowest spherical-harmonic degree considered is 16. Purucker
 335 et al. (2002) have argued that the large anomalies in southern North America could be the edge
 336 effects of large-scale cratonic magnetisation which is not contained in truncated lithospheric field
 337 models. In this paper we can not study magnetisation of the continents or the oceans, only the
 338 magnetic field itself and how it is expressed over the individual domains.

339 3.1 Decomposition using low-pass Slepian functions

340 From the MF7 model we use the first 5328 Gauss coefficients (up to degree and order 72) and
 341 include the g_0^0 coefficient (set to zero, as are degrees 1–15) for the purposes of the Slepian decom-
 342 position. A symmetric (5329×5329) localisation matrix \mathbf{D} of eq. (14) is computed from a list
 343 of 10151 (latitude, longitude) pairs representing the continental shelf boundary, closed by spline

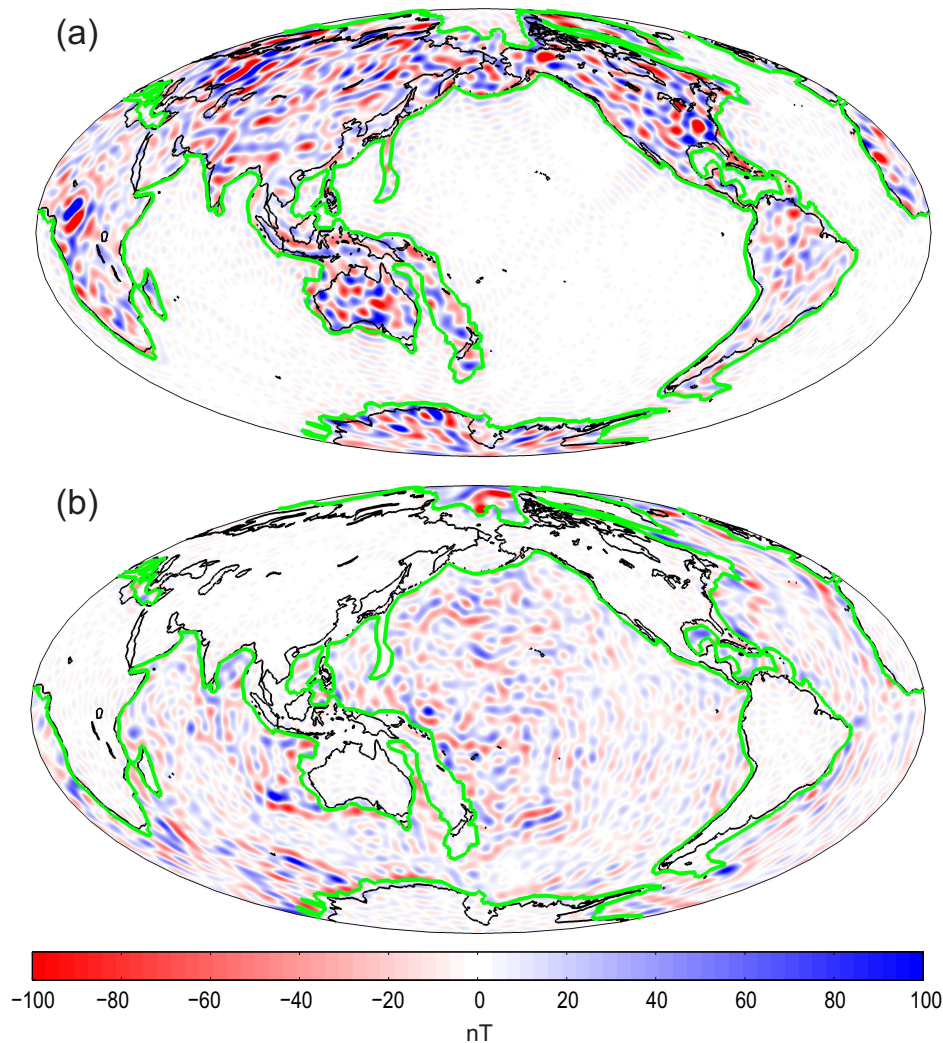


Figure 2. The radial component of the MF7 magnetic field data decomposed into (a) continental and (b) oceanic signals (units: nT). This decomposition uses low-pass Slepian functions that include spherical-harmonic degrees 0–72, although the input model contains only degrees 16–72. The separation of the basis set happens at the Shannon number, $K = 2170$ for the continents, which leaves 3159 functions to approximate the signal over the oceans.

344 interpolation. The eigenvectors of the localisation matrix are sorted by decreasing eigenvalue and
 345 then the Gauss coefficients are converted into the equivalent complete description by Slepian func-
 346 tion coefficients.

347 Fig. 2 shows the radial components of the continental and the oceanic signals expressed in the
 348 Slepian basis. In both cases, the signal outside the chosen area is very small, though in neither case
 349 does it vanish completely. Moreover, certain features generate systematic reverberation, or ringing,

350 in the adjacent regions — such as that of continental signal south of Australia (upper panel). The
351 computed Shannon number assigns 2170 Slepian basis functions to the continental crust and 3159
352 to the oceanic crust. Judging from the corresponding eigenvalues, about 5.0% of the energy of the
353 continental basis is outside of the boundaries; while for the oceanic basis, some 3.4% leaks into
354 the continental domain. From a spatial integration of the original signal and its comparison to the
355 reconstruction over the partial domains, more than 98.2% of the energy of the spatial signal is
356 recovered in the continents, while 94.9% is recovered over the oceans.

357 Fig. 3 shows the power spectra of the decomposed signals. In using eq. (5) for the computations
358 in the case of the decomposed fields, we continue to refer to the surface area of the entire sphere,
359 even though we have effectively zeroed out the contributions from the regions outside those of
360 interest. A different definition of “power” spectrum might have scaled our results by the areas
361 of the region of interest. On the other hand, a different interpretation of our computations might
362 thus interpret our comparative results as “energy” spectra rather than power spectra. Whatever the
363 preference of the reader, the computer code that accompanies this paper can be easily adapted to
364 make accommodations for taste.

365 For the oceanic region, degree 16 and the highest degrees (around 70) stand out. Degree 16
366 corresponds approximately to a wavelength of 2500 km, possibly present in the (north–south)
367 direction parallel to the mid-ocean ridges. Degree 70 corresponds approximately to wavelengths
368 of 550 km, which is perhaps the longitudinal wavelength of the north-south oriented magnetic
369 “stripes” visible by satellites in the Atlantic basin. The spectrum of the continental region shows
370 much more variability than the oceanic signal. There are many peaks that follow those of the global
371 spectrum. The peak at degree 25 is present in the oceanic signal but otherwise the large peaks are
372 limited to the continents. Overall, the power from the continental region is significantly greater
373 than the power of the oceanic region. This is most likely owing to the larger volume of magnetic
374 rocks in the continents despite their smaller areal extent.

375 Fig. 3 also shows explicitly that the power spectrum of the sum of the decomposed signals is
376 identical to the global spectrum of the original, while it can be shown that the sum of the partial
377 spectra is a good, though not perfect, approximation to the global spectrum. We also see that there

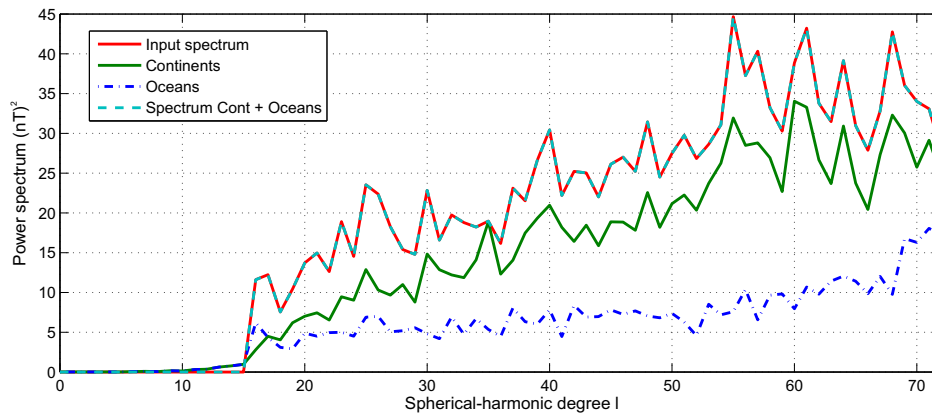


Figure 3. Power spectra of the crustal magnetic field MF7, globally (“input”), and with the signals decomposed into continental and oceanic domains using low-pass Slepian functions that contain all spherical-harmonic degrees from 0–72. Also shown is the spectrum of the sum of the continent and ocean model fields, which is a close approximation to the global spectrum. Units: nT^2 .

378 is some spectral leakage into the degrees below 16, though this is quite low compared to the power
 379 elsewhere. At this point, we also note that we have decomposed other lithospheric field models
 380 including MF6 (Maus et al. 2008) and POMME (Maus et al. 2010) which gave similar results to
 381 those shown in Figs. 2 and 3.

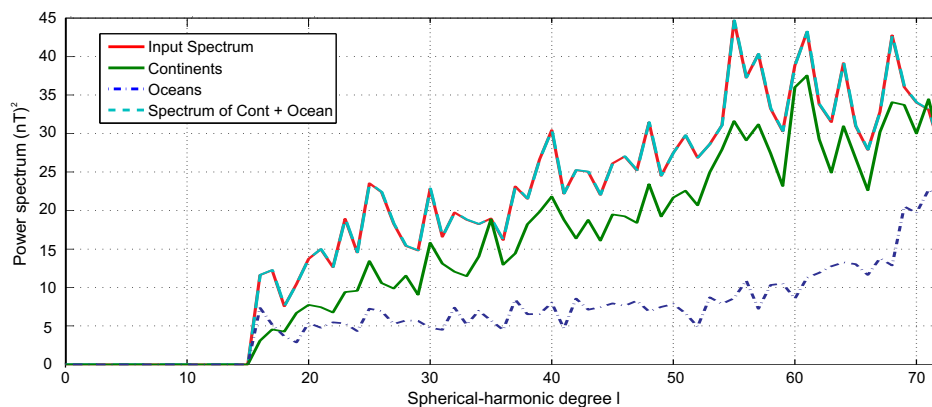


Figure 4. Power spectra of the crustal magnetic field MF7, globally, and with the signals decomposed using band-pass Slepian functions that contain only spherical-harmonic degrees between 16–72, and the spectrum of the sum of the decomposed model fields, as described in the text. Units: nT^2 .

3.2 Decomposition using band-pass Slepian functions

Fig. 4 shows the power spectra for the model decomposed in band-pass Slepian functions of degrees $l = 16\text{--}72$. The results are similar to the low-pass $l = 0\text{--}72$ decomposition shown in Fig. 3. Spatial leakage is slightly more prominent than previously, as deduced from the eigenvalues of the solution: 5.7% of energy out of the continental basis and 3.6% from the oceanic basis. At the North pole the leakage of continental signal is more pronounced, though overall the spatial leakage is still quite small. In the oceanic spectrum, the peak at degree 16 is stronger than for the low-pass Slepian functions, since with the band-pass functions coupling to the degrees 0–15 is excluded. There are also power increases at higher degrees.

3.3 Individual continents and ocean basins

We next decompose the field model MF7 into five continental areas — Americas (North, Central and South), Africa, Eurasia, Australia and Antarctica — and four ocean basins — Atlantic, Pacific, Indian and North Pole. The field over each decomposed region is calculated from the original MF7 magnetic potential model (not from the decomposed components of the previous sections). Each time, the separation was performed using the appropriate Shannon number for the area under consideration.

Fig. 5 shows the power spectra of the decomposed regions. The sum of the partial spectra for these nine parts approximates very well, but does not exactly match, the global MF7 spectrum. There are similar contrasts between continental and oceanic signals as noted previously. For instance, continental spectra seem to “flatten” towards the highest harmonic degrees, while the oceanic spectra tend to start to increase at higher degrees. There is much greater roughness in the spectra of the continental regions than in those of the oceanic ones. Eurasia and Americas, in particular, show most departure from a smooth curve, exhibiting a series of crests and troughs in their spectra. The spectrum of the Americas contains one prominent peak close to degree 60 whereas that of Eurasia contains at least three peaks and displays overall much greater power within the degree range 50–70 than any other continental region. All of the continental regions are characterised by power that diminishes significantly from the higher to the lower degrees.

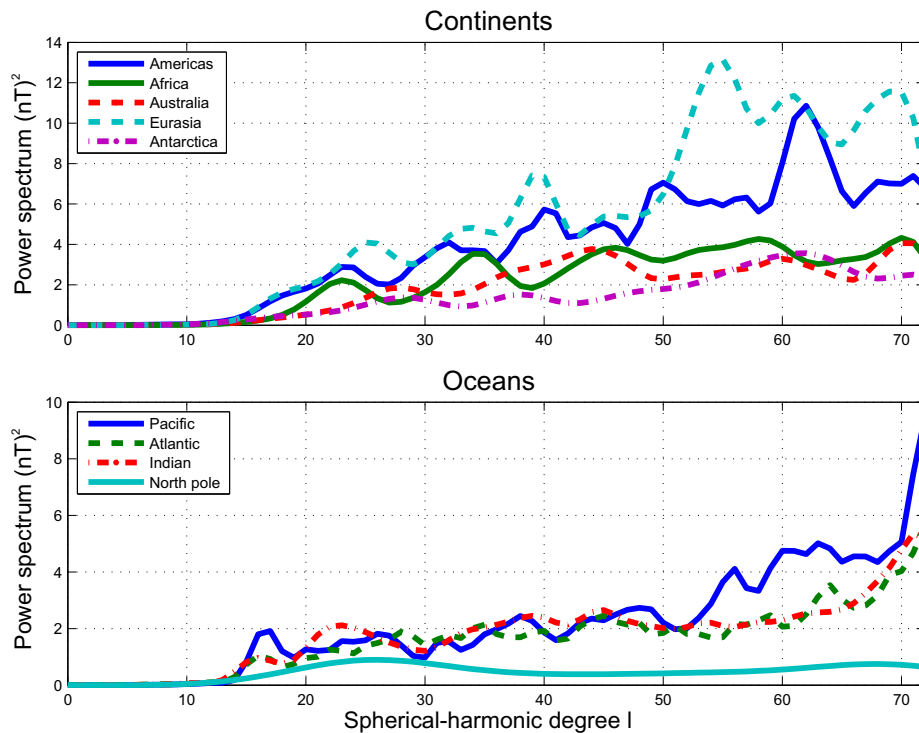


Figure 5. The power spectrum of the crustal magnetic field decomposed into nine different regions. Continental regions are presented in the upper plot and oceanic regions are in the lower one. The sum of the partial spectra is a very good approximation to the global spectrum. Units: nT^2 .

409 In the oceanic signals, only the Pacific spectrum contains a clear peak at degree 16, which
 410 was noticeable in the all-oceanic signal shown in Fig. 3. Hence, whatever the cause of this long-
 411 wavelength variation, it most likely originates in the Pacific Ocean. The Pacific Ocean spectrum
 412 also exhibits much more variability than that of other oceanic regions. However, it does not account
 413 for much greater power than the spectra of the Atlantic or Indian Oceans, although its area is twice
 414 as large. There are also differences in smoothness of the spectra. The Pacific and Atlantic Ocean
 415 spectra are much less smooth than those for most of the continental regions, except for that of the
 416 Americas which also exhibits abrupt changes in slope. The North Pole is included in the oceanic
 417 areas, but it is questionable whether it is possible to obtain any information from the area by this
 418 analysis, as the area of the region is less than 1% of the whole globe and it lies within the satellite
 419 polar gap. Thus it is unlikely to have significant information or power at any of the wavelengths
 420 analysed here.

421 3.4 Spectral coupling in the decomposed signals

422 Quantifying the spectral coupling or leakage within a decomposed signal allows us to determine
 423 the resolution of our power-spectral results. The coupling is related to the size of the region of
 424 interest, its shape, the degree resolution of the model, and the truncation level of the bases. Cou-
 425 pling between degrees and orders arises from the separation of the matrix \mathbf{G}^T that we encoun-
 426 tered in eq. (11), which breaks its unitarity. Summation over the orders in the squared $\mathbf{G}_{\text{in}}\mathbf{G}_{\text{in}}^T$ and
 427 $\mathbf{G}_{\text{out}}\mathbf{G}_{\text{out}}^T$ projection matrices quantifies the spectral coupling between individual degrees in the
 428 power-spectral estimate of eq. (5) made with Gauss coefficients transformed via eqs (22)–(23),
 429 and by analogy with properties of spectral estimators discussed by Dahlen & Simons (2008, their
 430 eqs 57, 131 and 140). For example, the spectral coupling matrix $\mathbf{C}_{\text{in}} = (\mathbf{G}_{\text{in}}\mathbf{G}_{\text{in}}^T)^2$ for the “in”
 431 region yields a $(73^2 \times 73^2)$ matrix. The coupling value for each degree l is computed by summing
 432 over the orders of \mathbf{C}_{in} , and dividing by $(2l + 1)$, resulting in a (73×73) matrix. Ideally, these
 433 summation matrices should closely approximate the identity matrix, indicating a lack of coupling
 434 between degrees (but remember that eq. 5 contains a sum over the orders), but such a situation is
 435 not generally achievable when regional resolution over partial spatial domains is being sought.

436 Fig. 6 shows the values of the coupling matrices for low-pass degree 0–72 Slepian functions
 437 with Shannon-number truncation. The behaviour of the band-pass functions is qualitatively similar
 438 and will not be illustrated here. The coupling is plotted on a logarithmic scale to emphasise the
 439 detail in the matrices. Coupling is evident between degrees 0–15 which accounts for the spectral
 440 leakage seen in Fig. 3. From degrees 16–72 the coupling of both regions shows a strong peak at the
 441 central degree, with narrow flanks. The lower panel of Fig. 6 shows the coupling of degree $l = 36$
 442 for the continental “in” and oceanic “out” domains (i. e. the 37th row of the low-pass coupling
 443 matrices). There is a strong peak at the target degree, with narrow shoulders falling to approxi-
 444 mately zero at about six spherical-harmonic degrees on either side. Except at the low-degree and
 445 high-degree edges of the domain, the coupling matrices are roughly constant-diagonal, which im-
 446 plies that in the interior the bandwidth of our spectral estimate is about twelve spherical-harmonic
 447 degrees. The effective bandwidth, in terms of its full-width at half height, is much smaller than
 448 that, only about two to three degrees. Information from degrees outside this band does not couple

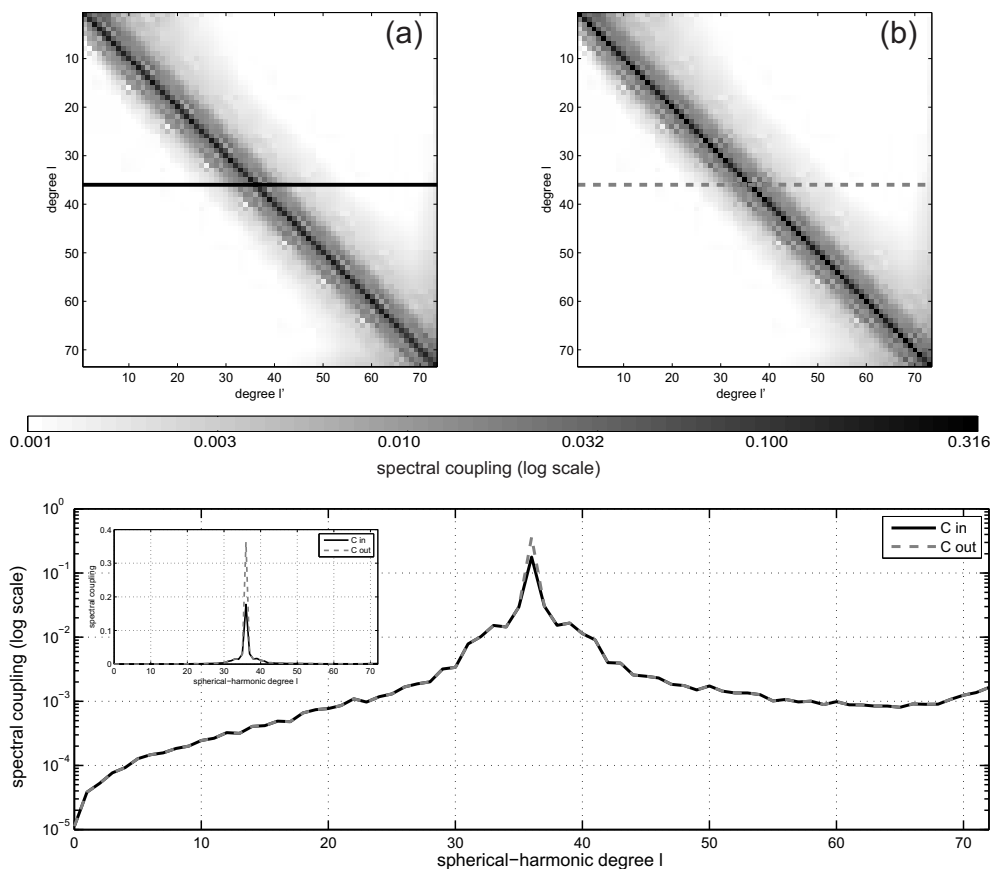


Figure 6. Coupling matrices for the spherical-harmonic power spectrum of the domain-decomposed fields. (a) Coupling when using $K = 2170$ Slepian functions to concentrate over the continents, and (b) when using $(L - 1)^2 - K = 3159$ Slepian functions over the oceans. The values shown at each degree contain the normalisation factor $(2l + 1)$, as defined in Section 3.4. The lower panel shows the coupling of degree $l = 36$ of the continental (solid black) and oceanic (dashed grey) decomposition, on a log scale. A linear plot of the same data is shown in the left-hand corner.

449 strongly into the spectral estimate of the decomposed fields at the target. A comparison of this cou-
 450 pling with the behaviour of the “periodogram” and “(multi-)taper” estimates, derived and depicted
 451 by Dahlen & Simons (2008, their Figs 4–7), illustrates that the method employed in this paper is
 452 an effective way of localising the power spectral estimate both in the spatial and spectral domains.

453 To give a visual sense of how spectral coupling works under our procedure, we illustrate it by
 454 simply decomposing models containing only one or a few individual spherical-harmonic degrees
 455 at a time. Using only coefficients from one spherical-harmonic degree (and including all orders
 456 of that degree) of the global model, we decompose it into oceanic and continental regions. The
 457 first such experiment is shown in Fig. 7(a). We then progressively add one extra model degree at

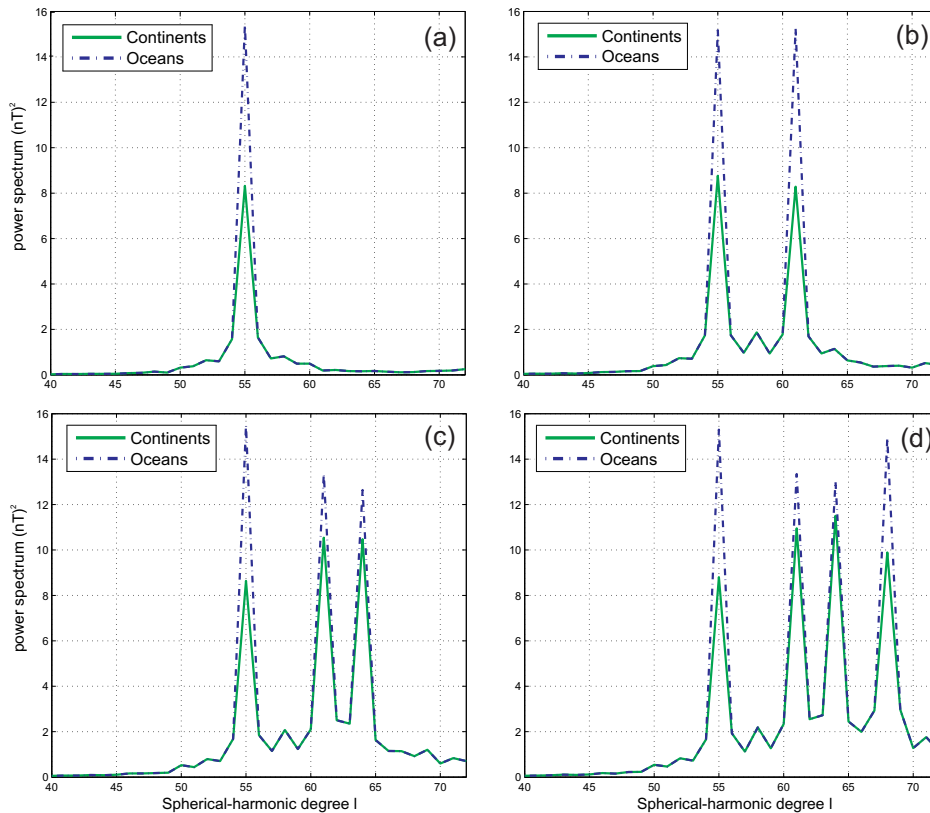


Figure 7. Decomposing strong peaks in the MF7 spectrum into oceanic and continental signals. These are taken at the four peaks in the global spectrum within degrees 55–68. First the data of (a) one peak ($l = 55$), then the data of (b) two peaks ($l = 55$ and 61), then (c) three peaks ($l = 55$, 61 and 64) and finally (d) all four peaks ($l = 55$, 61 , 64 and 68) are analysed. Units: nT^2 .

458 a time, successively decomposing these synthesised fields into continental and oceanic parts, and
 459 calculating the power spectrum, as shown in Fig. 7(b)–(d). The four spherical-harmonic degrees
 460 are chosen from the higher end of the spectrum where continental crust dominates, specifically
 461 degrees 55, 61, 64 and 68, where prominent peaks were seen to occur in Fig. 3.

462 Fig. 7 shows the spectra of these decomposed signals. The peaks as recovered relate to the
 463 input power spectrum via convolution with the spectral coupling matrices of Fig. 6, as first shown
 464 by Wieczorek & Simons (2005, 2007) and generalised by Dahlen & Simons (2008, their eqs 59,
 465 135 and 140). Thus, the result for the single spike in Fig. 7(a) is similar to the curves from the
 466 cross-section of the coupling matrices in Fig. 6. As our spectral mean squares refer to the whole
 467 sphere, and not just to the area of the continents or oceans, due to its greater area, the power
 468 spectrum in the oceanic signal is greater than that of the continents. If instead of the low-pass

469 Slepian functions, their band-pass versions are being used, all relationships between degrees are
470 altered, but the procedure for their evaluation remains identical. The spectral coupling matrix
471 contains the information on the blurring that is caused by the particular decomposition, and spike
472 tests can be performed for visual guidance. The band-pass and low-pass Slepian-function model
473 decompositions are different. Since the crustal-field model does not contain the lowermost degrees,
474 neither should the decomposed signals. For this reason, we prefer the analysis using the band-
475 passed Slepian functions, although Figs 3–4 show that the interpretative differences will be minor.

476 When the power spectrum shows significant roughness, or when the spectrum has a local slope
477 that is significantly different from zero (indicating a “non-flat” spectral process), the coupling be-
478 tween spherical-harmonic degrees induced by the decomposition will lead to estimates that are
479 significantly biased, as they would be with any other partial-domain method (Dahlen & Simons
480 2008). In contrast, the spectral estimates for smoothly-varying, flat or “moderately coloured” spec-
481 tra will be approximately unbiased, if properly scaled. The interpretation of what constitutes “mod-
482 erate” colouring is to be made with reference to the effective bandwidth of the spectral estimator.
483 The comparison of the global power spectra in Figs 3–4 with the effective bandwidth of the esti-
484 mator, as apparent from Fig. 6, suggests that this interpretative approximation is justified. We thus
485 conclude that the decomposition of the global crustal magnetic field using Slepian functions into
486 oceanic and continental portions not only provides an excellent approximation to the individual
487 fields in the space domain, but also leads to useful and reliable representations of their power spec-
488 tra. A complete multitaper analysis in the vein of Dahlen & Simons (2008, their Section 7) would
489 provide more control over the variance of the power-spectral estimate, but given the clear-cut spec-
490 tral separation of the source model after the spatial decomposition in the case of the magnetic field,
491 the benefits would be largely statistical. However, should the spectrum need to be known with its
492 uncertainty in order to map this into uncertainties on model parameters derived from it, such an
493 approach might still be preferable, as shown by Lewis & Simons (2012) for the Martian magnetic
494 field.

4 DISCUSSION

In this work we employed spatio-spectrally concentrated spherical Slepian functions to decompose global geomagnetic models, available as spherical-harmonic expansion coefficients, into their regional contributions. Our experiments with the terrestrial lithospheric field indicate that there is a clear difference between the magnetic signature of continents versus oceans, and provide a quantitative basis for its interpretation.

First, the continental field carries more than twice as much energy (mean-squared field over the sphere summed over all available harmonics, defined in eq. 5) as the oceanic field, although the continental area is only $\sim 40\%$ of the surface. This can be explained by the larger volume of the continental crust, although it should be counter-balanced to some extent by extrusive oceanic basaltic layers with strong magnetisation (Purucker et al. 2003; Gubbins et al. 2011). Second, the oceanic signal contains approximately equal total power at all degrees, whereas the shape of the continental power spectrum resembles that of the whole field (increasing towards higher degrees and flattening slightly towards the end).

The oceanic spectrum arises from a combination of processes, some natural and some inherent in the data processing, such as randomly timed reversals of magnetic poles, non-uniform plate motions and the smoothing effect of the satellite measurements from which MF7 is derived. We conclude that the young, steadily regenerating oceanic crust contains approximately equal power over all degrees, whereas the more mature, slowly evolving, crust of the continents possesses significantly more power in the higher degrees, due to the thickness of the continents and the nature of their amalgamation.

As an additional experiment, we decomposed the historical core field of the model *gufm1* at the CMB (Jackson et al. 2000) into regions of anomalously slow seismic shear wave velocities and their complement (Grand 2002). These decompositions were produced for every 10 years for the time period 1590–1990, with the results indicating that, approaching the present date, the spectral signatures of the decomposed regions become increasingly indistinct, suggesting that few unambiguously resolvable differences exist between them. However, we concluded from examination of the coupling matrices that when the range of spherical harmonics degrees is limited, such as is

523 the case with the core field, the spatio-spectral decomposition is not sufficiently discriminant to
524 justify strong conclusions.

525 **5 CONCLUSIONS**

526 Using spherical Slepian functions, both in their traditional low-pass (for the degrees 0–72) and
527 novel band-pass (for degrees 16–72) incarnations, we decomposed the global lithospheric mag-
528 netic field model MF7, complete to spherical-harmonic degree and order 72, into two regions: one
529 that is localised over the continents, and its complement which is localised in the ocean basins. The
530 results demonstrate that the continental region dominates the lithospheric magnetic field, and also
531 that the two regions have very distinct spectral signatures. The oceanic signal appears to have ap-
532 proximately equal power across all spherical-harmonic degrees while the continental signal shows
533 increasing power as a function of degree.

534 Our method provides interpretable decompositions when the data set has a smoothly varying
535 spectrum (with respect to the effective coupling bandwidth of the spectral estimate) and when
536 the range of spherical harmonics degrees is sufficiently large. The lithospheric field was a prime
537 candidate for our analysis; in contrast, the core field does not meet these criteria.

538 The analysis using Slepian functions is one of a range of localisation methods that are ap-
539 plicable to a large number of (geophysical) studies where spherical-harmonic modelling is used.
540 The key advantages of Slepian functions are their harmonicity and double orthogonality, both
541 over the region of interest and over the whole sphere, their ease of calculation, and their possi-
542 ble application as basis functions to conduct linear inverse problems, or as windowing functions
543 to perform quadratic spectral analysis. Each of those aspects has received a thorough theoretical
544 treatment in prior work. The method developed in this paper represents a hybrid form, whereby
545 we approximated the signal of interest inside of the individual regions of study using a truncated
546 Slepian expansion, and subsequently, we employed the traditional Mauersberger-Lowes spherical-
547 harmonics-based power-spectral estimation on the space-domain results. We have shown how this
548 resulted in appropriately spatio-spectrally concentrated estimates both of the underlying signals

549 and their power spectra, and we showed how to interpret the resolution of the resultant spectral
550 estimate via a characterisation of its coupling (or leakage) kernel.

551 **ACKNOWLEDGMENTS**

552 We sincerely thank the Editor, Richard Holmes, Erwan Thébault, and Frank Lowes, for their pa-
553 tience, their support, and the detailed commentary on two earlier versions of this manuscript. This
554 research was partly funded by the NERC GEOSPACE programme under grants NER/O/S/2003/00674
555 and NER/O/S/2003/00677, and published with the permission of the Executive Director of the
556 British Geological Survey (NERC). We acknowledge the use of the ETOPO2v2 map from the
557 National Oceanic and Atmospheric Administration, National Geophysical Data Center, USA. FJS
558 thanks the U. S. National Science Foundation for support under CAREER grant EAR-1150145,
559 and Princeton University account 195-2243. Computer code to perform the analysis and generate
560 the figures in this paper is available from <http://www.frederik.net>.

561 **REFERENCES**

- 562 Amirbekyan, A., Michel, V., & Simons, F. J., 2008. Parameterizing surface-wave tomographic
563 models with harmonic spherical splines, *Geophys. J. Int.*, **174**(2), 617–628, doi: 10.1111/j.1365-
564 246X.2008.03809.x.
- 565 Arkani-Hamed, J. & Dyment, J., 1996. Magnetic potential and magnetization contrasts of Earth's litho-
566 sphere, *J. Geophys. Res.*, **101**(B5), 11401–11411.
- 567 Backus, G. E., Parker, R. L., & Constable, C. G., 1996. *Foundations of geomagnetism*, Cambridge
568 Univ. Press, Cambridge, UK.
- 569 Becker, T. W. & Boschi, L., 2002. A comparison of tomographic and geodynamic mantle models,
570 *Geochem. Geophys. Geosys.*, **3**(1), 1003, doi: 10.1029/2001GC000168.
- 571 Blakely, R. J., 1996. *Potential theory in gravity and magnetic applications*, Cambridge University Press.
- 572 Cohen, Y. & Achache, J., 1994. Contribution of induced and remanent magnetization to long-wavelength
573 oceanic magnetic anomalies, *Journal of Geophysical Research*, **99**(B2), 2943–2954.
- 574 Counil, J. L., Cohen, Y., & Achache, J., 1991. The global continent-ocean magnetization contrast, *Earth*
575 *Planet. Sci. Lett.*, **103**(1-4), 354–364.
- 576 Dahlen, F. A. & Simons, F. J., 2008. Spectral estimation on a sphere in geophysics and cosmology,
577 *Geophys. J. Int.*, **174**, 774–807, doi: 10.1111/j.1365-246X.2008.03854.x.

- 578 Daubechies, I., 1992. *Ten Lectures on Wavelets*, vol. 61 of **CBMS-NSF Regional Conference Series in**
579 **Applied Mathematics**, Society for Industrial & Applied Mathematics, Philadelphia, Penn.
- 580 Dymont, J. & Arkani-Hamed, J., 1998. Contribution of lithospheric remanent magnetization to satellite
581 magnetic anomalies over the world's oceans, *J. Geophys. Res.*, **103**, 15423–15441.
- 582 Freedon, W. & Michel, V., 1999. Constructive approximation and numerical methods in geodetic research
583 today – an attempt at a categorization based on an uncertainty principle, *J. Geodesy*, **73**(9), 452–465.
- 584 Friis-Christensen, E., Lühr, H., & Hulot, G., 2006. Swarm: A constellation to study the Earth's magnetic
585 field, *Earth Planets Space*, **58**, 351358.
- 586 Górski, K. M., 1994. On determining the spectrum of primordial inhomogeneity from the COBE DMR
587 sky maps – Method, *Astroph. J.*, **430**(2), L85–L88.
- 588 Grand, S., 2002. Mantle shear-wave tomography and the fate of subducted slabs, *Phil. Trans. Royal Soc.*
589 *London. A*, **360**(1800), 2475–2491.
- 590 Gubbins, D., Ivers, D., Masterton, S. M., & Winch, D. E., 2011. Analysis of lithospheric magnetization in
591 vector spherical harmonics, *Geophys. J. Int.*, **187**, 99–117, doi: 10.1111/j.1365–246X.2011.05153.x.
- 592 Haines, G., 1985. Spherical cap harmonic analysis, *J. Geophys. Res.*, **90** (B3), 2583–2591.
- 593 Harig, C. & Simons, F. J., 2012. Mapping Greenland's mass loss in space and time, *Proc. Natl. Acad. Sc.*,
594 pp. in the press, doi: 10.1073/pnas.1206785109.
- 595 Hauser, M. G. & Peebles, P. J. E., 1973. Statistical analysis of catalogs of extragalactic objects. II. The
596 Abell catalog of rich clusters, *Astroph. J.*, **185**, 757–785.
- 597 Hipkin, R. G., 2001. The statistics of pink noise on a sphere: applications to mantle density anomalies,
598 *Geophys. J. Int.*, **144**, 259–270.
- 599 Holschneider, M., Chambodut, A., & Manda, M., 2003. From global to regional analysis of the magnetic
600 field on the sphere using wavelet frames, *Phys. Earth Planet. Int.*, **135**, 107124.
- 601 Hulot, G., Finlay, C., Constable, C., Olsen, N., & Manda, M., 2010. The Magnetic Field of Planet Earth,
602 *Space Sci. Rev.*, **152**, 159–222.
- 603 Hwang, C., 1993. Spectral analysis using orthonormal functions with a case study on sea surface topogra-
604 phy, *Geophys. J. Int.*, **115**, 1148–1160.
- 605 Jackson, A., Jonkers, A., & Walker, M., 2000. Four centuries of geomagnetic secular variation from
606 historical records, *Phil. Trans. R. Soc. London. A*, **358**(1768), 957–990, Mathematical, Physical and En-
607 gineering Sciences.
- 608 Jolliffe, I. T., 2002. *Principal component analysis*, Springer, 2nd edn.
- 609 Kaula, W. M., 1967. Theory of statistical analysis of data distributed over a sphere, *Rev. Geophys.*, **5**(1),
610 83–107.
- 611 Kono, M., 2007. Geomagnetism in Perspective, in *Treatise on Geophysics*, vol. 5, pp. 1–31, ed. Schubert,
612 G., Elsevier.

- 613 Langel, R. A. & Hinze, W. J., 1998. *The magnetic field of the Earth's lithosphere: the satellite perspective*,
614 Cambridge University Press.
- 615 Lesur, 2006. Introducing localized constraints in global geomagnetic field modelling, *Earth Planets Space*,
616 **58**, 477–483.
- 617 Lewis, K. W. & Simons, F. J., 2012. Local spectral variability and the origin of the Martian crustal
618 magnetic field, *Geophys. Res. Lett.*, **39**, L18201, doi: 10.1029/2012GL052708.
- 619 Lowes, F. J., 1966. Mean-square values on sphere of spherical harmonic fields, *J. Geophys. Res.*, **71**(8),
620 2179.
- 621 Lowes, F. J., 1974. Spatial power spectrum of the main geomagnetic field, and extrapolation to the core,
622 *Geophys. J. Royal Astr. Soc.*, **36**(3), 717–730.
- 623 Mallat, S., 1998. *A Wavelet Tour of Signal Processing*, Academic Press, San Diego, Calif.
- 624 Mauersberger, P., 1956. Das Mittel der Energiedichte des geomagnetischen Hauptfeldes an der Er-
625 doberfläche und seine säkulare Änderung, *Gerlands Beitr. Geophys.*, **65**, 207–215.
- 626 Maus, S., 2008. The geomagnetic power spectrum, *Geophys. J. Int.*, **174**, 135–142.
- 627 Maus, S., Lühr, H., Rother, M., Hemant, K., Balasis, G., Ritter, P., & Stolle, C., 2007. Fifth-generation
628 lithospheric magnetic field model from CHAMP satellite measurements, *Geochem. Geophys. Geosys.*,
629 **8**(5), Q05013.
- 630 Maus, S., Yin, F., Lühr, H., Manoj, C., Rother, M., Rauberg, J., Michaelis, I., Stolle, C., & Müller, R. D.,
631 2008. Resolution of direction of oceanic magnetic lineations by the sixth-generation lithospheric mag-
632 netic field model from champ satellite magnetic measurements, *Geochem. Geophys. Geosyst.*, **9**, Q07021.
- 633 Maus, S., Barckhausen, U., Berkenbosch, H., Bournas, N., Brozena, J., Childers, V., Dostaler, F., Fairhead,
634 J. D., Finn, C., von Frese, R. R. B., Gaina, C., Golynsky, S., Kucks, R., Lühr, H., Milligan, P., Mogren,
635 S., Müller, D., Olesen, O., Pilkington, M., Saltus, R., Schreckenberger, B., Thébault, E., & Tontini, F. C.,
636 2009. EMAG2: A 2-arc min resolution Earth Magnetic Anomaly Grid compiled from satellite, airborne,
637 and marine magnetic measurements, *Geochem. Geophys. Geosyst.*, **10**, Q08005.
- 638 Maus, S., Manoj, C., Rauberg, J., Michaelis, I., & Lühr, H., 2010. NOAA/NGDC candidate models for
639 the 11th generation International Geomagnetic Reference Field and the concurrent release of the 6th
640 generation Pomme magnetic model, *Earth Planet. Space*, **62**, 729–735.
- 641 Müller, R., Sdrolias, M., Gaina, C., & Roest, W., 2008. Age, spreading rates, and spreading asymmetry of
642 the world's ocean crust, *Geochem. Geophys. Geosys.*, **9**(5), Q04006.
- 643 Narcowich, F. J. & Ward, J. D., 1996. Nonstationary wavelets on the m-sphere for scattered data,
644 *Appl. Comput. Harmon. Anal.*, **3**, 324–336.
- 645 Oh, S. P., Spergel, D. N., & Hinshaw, G., 1999. An efficient technique to determine the power spectrum
646 from cosmic microwave background sky maps, *Astroph. J.*, **510**, 551–563.
- 647 Peebles, P. J. E., 1973. Statistical analysis of catalogs of extragalactic objects. I. Theory, *Astroph. J.*, **185**,

648 413–440.

649 Percival, D. B. & Walden, A. T., 1993. *Spectral Analysis for Physical Applications, Multitaper and Con-*
 650 *ventional Univariate Techniques*, Cambridge Univ. Press, New York.

651 Plattner, A. & Simons, F. J., 2012. Spatiospectral concentration of vector fields on a sphere, *Appl. Com-*
 652 *put. Harmon. Anal.*, p. in revision.

653 Plattner, A., Simons, F. J., & Wei, L., 2012. Analysis of real vector fields on the sphere using Slepian
 654 functions, in *2012 IEEE Statistical Signal Processing Workshop (SSP'12)*, IEEE.

655 Purucker, M., Langlais, B., Olsen, N., Hulot, G., & Manda, M., 2002. The southern edge of cratonic
 656 North America: Evidence from new satellite magnetometer observations, *Geophys. Res. Lett.*, **29**(15),
 657 8000–8003.

658 Purucker, M., Sabaka, T., Olsen, N., & Maus, S., 2003. How have Ørsted, CHAMP, and SAC-C im-
 659 proved our knowledge of the oceanic regions?, in *Proceedings of the 4th OIST conference*, Copenhagen,
 660 Denmark.

661 Reigber, C., Schmidt, R., Flechtner, F., König, R., Meyer, U., Neumayer, K.-H., Schwintzer, P., & Zhu, S.,
 662 2005. An Earth gravity field model complete to degree and order 150 from GRACE: EIGEN-GRACE02S,
 663 *J. Geodyn.*, **39**, 1–10.

664 Ritsema, J., A. Deuss, A., van Heijst, H. J., & Woodhouse, J. H., 2010. S40RTS: a degree-40 shear-velocity
 665 model for the mantle from new Rayleigh wave dispersion, teleseismic traveltime and normal-mode split-
 666 ting function measurements, *Geophys. J. Int.*, **184**, 1223–1236, doi: 10.1111/j.1365–246X.2010.04884.x.

667 Sabaka, T. J., Hulot, G., & Olsen, N., 2010. Mathematical properties relevant to geomagnetic field model-
 668 ing, in *Handbook of Geomathematics*, chap. 17, pp. 503–538, doi: 10.1007/978–3–642–01546–5_17, eds
 669 Freeden, W., Nashed, M. Z., & Sonar, T., Springer, Heidelberg, Germany.

670 Schachtschneider, R., Holschneider, M., & Manda, M., 2010. Error distribution in regional inversion of
 671 potential field data, *Geophys. J. Int.*, **181**, 1428–1440, doi: 10.1111/j.1365–246X.2010.04598.x.

672 Schachtschneider, R., Holschneider, M., & Manda, M., 2012. Error distribution in regional modelling of
 673 the geomagnetic field, *Geophys. J. Int.*, **191**, 1015–1024, doi: 10.1111/j.1365–246X.2012.05675.x.

674 Schott, J. J. & Thébaud, E., 2011. Modelling the Earth's magnetic field from global to regional scales, in
 675 *Geomagnetic Observations and Models*, vol. 5 of **IAGA Special Sopron Book Series**, pp. 229–264, eds
 676 Manda, M. & Korte, M., Springer.

677 Shure, L., Parker, R. L., & Backus, G. E., 1982. Harmonic splines for geomagnetic modelling, *Phys. Earth*
 678 *Planet. Int.*, **28**, 215–229.

679 Shure, L., Parker, R. L., & Langel, R. A., 1985. A preliminary harmonic spline model from Magsat data,
 680 *J. Geophys. Res.*, **90**, 11505–11512.

681 Simons, F. J., 2010. Slepian functions and their use in signal estimation and spectral analysis, in *Handbook*
 682 *of Geomathematics*, chap. 30, eds Freeden, W., Nashed, M. Z., & Sonar, T., Springer.

- 683 Simons, F. J. & Dahlen, F. A., 2006. Spherical Slepian functions and the polar gap in geodesy, *Geo-*
684 *phys. J. Int.*, **166**, 1039–1061, doi: 10.1111/j.1365–246X.2006.03065.x.
- 685 Simons, F. J., Dahlen, F. A., & Wieczorek, M. A., 2006. Spatiospectral concentration on a sphere, *SIAM*
686 *Rev.*, **48**(3), 504–536, doi: 10.1137/S0036144504445765.
- 687 Simons, F. J., Hawthorne, J. C., & Beggan, C. D., 2009. Efficient analysis and representation of geophys-
688 ical processes using localized spherical basis functions, in *Wavelets XIII*, vol. 7446, pp. 74460G, doi:
689 10.1117/12.825730, SPIE.
- 690 Simons, M., Solomon, S. C., & Hager, B. H., 1997. Localization of gravity and topography: constraints
691 on the tectonics and mantle dynamics of Venus, *Geophys. J. Int.*, **131**, 24–44.
- 692 Slepian, D., 1983. Some comments on Fourier analysis, uncertainty and modeling, *SIAM Rev.*, **25**(3),
693 379–393.
- 694 Slobbe, D. C., Simons, F. J., & Klees, R., 2012. The spherical Slepian basis as a means to obtain spectral
695 consistency between mean sea level and the geoid, *J. Geodesy*, **86**(8), 609–628, doi: 10.1007/s00190–
696 012–0543–x.
- 697 Spencer, C. & Gubbins, D., 1980. Travel-time inversion for simultaneous earthquake location and velocity
698 structure determination in laterally varying media, *Geophys. J. R. Astron. Soc.*, **63**(1), 95–116.
- 699 Tegmark, M., 1996. A method for extracting maximum resolution power spectra from microwave sky
700 maps, *Mon. Not. R. Astron. Soc.*, **280**, 299–308.
- 701 Tegmark, M., 1997. How to measure CMB power spectra without losing information, *Phys. Rev. D*, **55**(10),
702 5895–5907.
- 703 Thébault, E., Schott, J. J., & Manda, M., 2006. Revised spherical cap harmonic analysis (RSCHA):
704 validation and properties, *J. Geophys. Res.*, **111**, B01102.
- 705 Thébault, E., Hemant, K., Hulot, G., & Olsen, N., 2009. On the geographical distribution of induced
706 time-varying crustal magnetic fields, *Geophys. Res. Lett.*, **36**, L01307.
- 707 Thébault, E., Purucker, M., Whaler, K. A., Langlais, B., & Sabaka, T. J., 2010. The magnetic field of the
708 Earth’s lithosphere, *Space Sci. Rev.*, pp. 1–33.
- 709 Thomson, A. W. P., Hamilton, B., Macmillan, S., & Reay, S. J., 2010. A novel weighting method for
710 satellite magnetic data and a new global magnetic field model, *Geophys. J. Int.*, **181**(1), 250–260.
- 711 Trampert, J. & Snieder, R., 1996. Model estimations biased by truncated expansions: Possible artifacts in
712 seismic tomography, *Science*, **271**(5253), 1257–1260, doi: 10.1126/science.271.5253.1257.
- 713 Wandelt, B. D., Hivon, E., & Górski, K. M., 2001. Cosmic microwave background anisotropy power
714 spectrum statistics for high precision cosmology, *Phys. Rev. D*, **64**(8), 083003.
- 715 Whaler, K. A. & Gubbins, D., 1981. Spherical harmonic analysis of the geomagnetic field: an example of
716 a linear inverse problem, *Geophys. J. Int.*, **65**(3), 645–693, doi: 10.1111/j.1365–246X.1981.tb04877.x.
- 717 Wieczorek, M. A. & Simons, F. J., 2005. Localized spectral analysis on the sphere, *Geophys. J. Int.*,

718 **162**(3), 655–675, doi: 10.1111/j.1365–246X.2005.02687.x.

719 Wieczorek, M. A. & Simons, F. J., 2007. Minimum-variance spectral analysis on the sphere, *J. Fourier*
720 *Anal. Appl.*, **13**(6), 665–692, doi: 10.1007/s00041–006–6904–1.

721 Xu, P., 1998. Truncated SVD methods for discrete linear ill-posed problems, *Geophys. J. Int.*, **135**(2),
722 505–514, doi: 10.1046/j.1365–246X.1998.00652.x.